Electron capture imaging of two-dimensional materials

G. Labaigt,[1,2] A. Dubois,[1,2] and J. P. Hansen[3]

[1]*Sorbonne Universités, UPMC Univ Paris 06, UMR 7614, Laboratoire de Chimie Physique-Matière et Rayonnement, F-75231, Paris, France*

[2]*CNRS, UMR 7614, LCPMR, 75005, Paris, France*

[3]*Department of Physics and Technology, University of Bergen, N-5007, Bergen, Norway*

(Received 16 January 2014; revised manuscript received 28 March 2014; published 24 June 2014)

We demonstrate that electron transfer induced by fast ion impact can be used as an imaging technique of two-dimensional materials. Applied to a keV proton beam passing through a graphene surface, it is shown that coherent single-electron capture gives a sub-ångström-scale spatial resolution image of the electronic structure of a single sheet. This imaging scheme is shown to be particularly effective, resolving missing atoms (vacancies) in the lattice, in a narrow projectile 5–10-keV energy region, where the capture probability exhibits a minimum at the center of the hexagonal cells. This geometry-dependent phenomenon is caused by the coupling dynamic between the initial state and a multi-electron entangled one-hole state and is therefore highly sample selective.

DOI: 10.1103/PhysRevB.89.245438 PACS number(s): 61.48.Gh, 34.70.+e, 68.37.−d

I. INTRODUCTION

Understanding the dynamic response of monolayer atomic surfaces to external perturbations requires methods from a variety of disciplines such as atomic, molecular, and (two-dimensional) condensed matter physics. Such materials, produced with tailored properties, possess a huge potential for applications. Graphene, a two-dimensional monolayer of C atoms, may in a future retrospect be seen as the "hydrogen atom" of monolayer systems and has, in recent years, been intensively studied for its extreme physical properties like strength and electronic conductivity [1]. Sheets of graphene can now routinely be suspended on boundaries [2], allowing for studies of atomic tunneling [3], molecular adsorption and charge transport [4], as well as internal properties of the graphene sheet itself [5].

The dynamic response of graphene to ultrafast and strong perturbations is still largely unexplored: Theoretical studies concerning strong laser fields interacting with graphene have recently indicated that higher and stronger harmonics are generated as compared to the harmonics from isolated C atoms [6]. At even higher laser intensities, the formation of a focused beam of relativistic electron has been predicted [7]. Regarding ion-impact, experiments with fast intense ion beams have displayed the radiation hardness of single and multiple graphene layers [8–11]. Another interesting scheme would be the study of the scattering of nondestructive ion beams at keV energies and below by a fixed graphene sheet. A multicenter coherent scattering theory, where the perpendicular beam profile may play an important role, will be required as the projectile ion will interact with a large number of surface atoms. New experimental setups may be envisioned as well, such as studies of coherent multiple excitation and deexcitation processes of a fixed graphene sheet from interactions with sequences of passing atoms analogous to experiments between Rydberg atoms interacting with photons in cavities [12].

For low-energy ion-impact the modeling has largely been performed based on the time-dependent density functional (TDDFT) method [13]. Using this approach [14] images of a single suspended graphene sheet were simulated for He^+ 30-keV impact, following the He ion microscope (HIM) scheme [15,16]. It was shown that the ion-induced electron emission from the sample is sensitive to the ion impact point, which allows atomic resolution of the surface.

In the present paper, we develop this idea in a different direction by showing the principle for a new sensitive camera for monolayer surface imaging based on electron transfer to the projectile processes instead of ionization processes, as in HIM. Since transfer (capture) processes are the dominant ones for low keV impact energies, are space localized, and largely limit the interaction with the sample, the use of electron capture imaging (ECI) scheme should provide bright images with high resolution as compared to techniques based on electron emission. From the experimental point of view the collision of charged projectiles with graphene in a perpendicular geometry (single sheet target) can be regarded as an ion-molecule collision so that the usual beam techniques, such as neutral or charged particle separation, detection, and energy analysis (i.e., time of flight) of atomic and molecular collision physics can be used for the imaging device, see, for example, Ref. [17]. Charge transfer is difficult to describe accurately based on TDDFT since the transfer probability is highly state selective in terms of projectile state energies, which within the TDDFT approach are known to depend on the local density [18]. Therefore we here develop a close-coupling semiclassical model using scattering states expressed as linear combinations of multicenter traveling atomic orbitals. In the limit of a single scattering center it reduces to well-known ion-atom scattering theory, which is Galilean invariant through the use of two-center basis states augmented by electron translational factors [19,20]. This dynamical approach allows for an exact quantification of the capture probabilities to each state of the projectile as well as a detailed map of the surface atom contribution to the charge transfer process.

In the paper we present our approach in detail as well as its implementation to describe the scattering of a proton beam perpendicular to a graphene sheet in the intermediate keV energy domain. We demonstrate the validity of the approach as well as the relevance of the proposed ECI scheme by presenting the convergence of the results with respect to the number of C atoms included in the calculations as

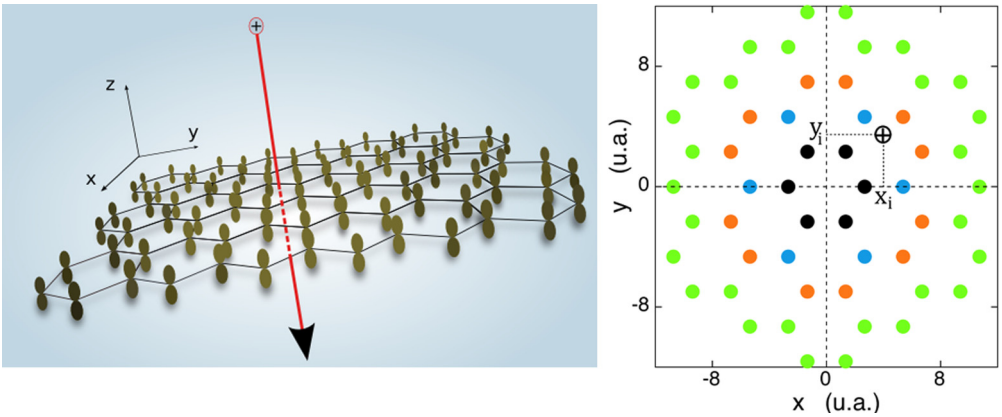

FIG. 1. (Color online) Left panel: Coordinate system and illustration of an H^+ ion passing through a graphene sheet. The highest occupied molecular orbital (HOMO) state of graphene is modeled by $2p_z$ Gaussian-type orbitals distributed on a honeycomb lattice in the xOy plane. Right panel: In the xOy graphene plane, the black circles represent $N = 6$ C sites and the blue, red, and green circles the extra sites for $N = 12$, 24, and 54 sites, respectively. A projectile impact point is marked on this plane and labeled by coordinates (x_i, y_i).

well as the impact energy dependence and selectivity of the capture probabilities. We finally propose a model to explain qualitatively the main features of the results, supporting that spatial and state-resolved measurements from a focused beam would reveal the surface electronic structure and the energy deposition on the surface and therefore provide the principle of a new type of imaging technique. Atomic units are used throughout unless stated otherwise.

II. THEORY

A. Model overview

In modeling the dynamics of the electron capture processes in the keV impact energy range, we approximate the projectile-target relative motion with the well-justified semiclassical impact parameter method, in the straight-line constant velocity approximation, i.e., $\mathbf{R}(t) = \mathbf{b} + \mathbf{v}\,t$ with the impact parameter $\mathbf{b}$ defined in the xOy graphene plane and the velocity $\mathbf{v}$ along the Oz axis, as illustrated in Fig. 1. The electronic dynamics is therefore described by the time-dependent Schrödinger equation

$$\left[\hat{\mathrm{H}} - i\frac{\partial}{\partial t}\right]\Psi(\mathbf{r}_1,\ldots,\mathbf{r}_N,t) = 0, \tag{1}$$

where the Hamiltonian $\hat{\mathrm{H}}$ of the multicenter multi-electron projectile-graphene scattering system will be approximated to handle the dynamics calculations. In our model, we include a necessary large number (N) of C atoms on the graphene sheet, localizing on each C center a unique electron, the outermost, less bound, one. The interaction between the electron and the ionic C center is therefore expressed in terms of a model potential taking into account the nucleus charge and the screening from the other (passive) electrons. This approximation is necessary, but also consistent with the rather small contribution of the lower-lying states of graphene to the capture processes at low keV energy [21,22]. Furthermore, we neglect multicenter electronic correlation and accordingly disregard multi-electronic and multicenter multi-electronic processes, such as double capture, capture-excitation, or electron hopping on the graphene sheet. Indeed these channels are expected to be much less probable in the considered impact energy domain, i.e., unlikely to happen in the subfemtosecond time scale where the electron transfer takes place.

B. Hamiltonian and basis set expansion

The N-electron Hamiltonian $\hat{\mathrm{H}}$ in Eq. (1) is then expressed as a sum of mono-electronic Hamiltonians $\hat{h}_i$

$$\hat{\mathrm{H}} = \sum_{i=1}^{N}\hat{h}_i = \sum_{i=1}^{N}\left[-\frac{1}{2}\nabla_i^2 + V_T\left(r_i^T\right) + V_P(|\mathbf{r}_i - \mathbf{R}(t)|)\right], \tag{2}$$

where V_P is the Coulombic potential with respect to the projectile and V_T a model potential which describes the interaction of the outermost electron and its C center, $\mathbf{r}_i^T = \mathbf{r}_i - \mathbf{q}_i$, with $\mathbf{q}_i$ the position of the C on the graphene plane. V_T is chosen to fulfill proper asymptotic conditions

$$V_T(r) = -\frac{1}{r} - \frac{5}{r}e^{-\alpha r^2} \tag{3}$$

and to bind the electron with an energy ε_0, in agreement with the ionization energy of graphene through the variational parameter α.

Within this model Eq. (1) is solved by expanding the total time-dependent N-electron wavefunction in terms of the initial state Φ_0 and a sum over capture-hole states Φ_j^{Tk}, as

$$\Psi(\mathbf{r}_1,\ldots,\mathbf{r}_N,t) = c_0(t)\,\Phi_0\,e^{-i\,N\varepsilon_0 t} + \sum_{k=1}^{N}\sum_{j=1}^{N_P} c_j^k(t)\,\Phi_j^{Tk} \times e^{i\{\mathbf{v}\cdot\mathbf{r}_k - [(N-1)\varepsilon_0 + E_j + \frac{1}{2}v^2]t\}}, \tag{4}$$

where k sums over the N C centers and j over the projectile states included in the calculations. More precisely, the initial state is expressed as a product of N $2p_z$ orbitals (labeled as ϕ^{Ti} in the following) centered at each atomic site and of energy ε_0

$$\Phi_0(\mathbf{r}_1,\ldots,\mathbf{r}_N) = \prod_{i=1}^{N}\phi^{Ti}\left(\mathbf{r}_i^T\right). \tag{5}$$

The final states Φ_j^{Tk} describe an electron in the state ϕ_j^P (of energy E_j) attached to the projectile with a corresponding hole at site k of the graphene sheet, the other N-1 electrons remain unchanged; it is then expressed as

$$\Phi_j^{Tk}(\mathbf{r}_1,\ldots,\mathbf{r}_N) = \phi_j^P(\mathbf{r}_k - \mathbf{R}) \prod_{i\neq k}^{N} \phi^{Ti}(\mathbf{r}_\mathbf{i}^\mathbf{T}). \tag{6}$$

Note that in Eq. (4) the projectile states are augmented by the usual electron translation factor (ETF) in the plane wave form to cancel spurious dipolar couplings and to ensure Galilean invariance of the results [19,23]. Finally, we neglect the overlaps between orbitals centered on neighboring sites, i.e., $\langle\phi^{Ti}|\phi^{Tj}\rangle = 0$ for $i \neq j$, as in the well-known Hückel method to describe π electrons in conjugated hydrocarbon planar structures, cf. Ref. [24].

The time-dependent Schrödinger equation, Eq. (1), is then solved as a set of ordinary first-order differential equations for the expansion coefficients $c(t)$ [$\equiv c_0(t)$ and $c_j^k(t)$] and expressed as

$$i\,S\frac{\partial}{\partial t}\,c = M\,c, \tag{7}$$

where S is the overlap matrix and M the coupling matrix for the operator $\hat{\mathrm{H}} - i\,\partial_t$. These two matrices have an identical block structure which can be schematized for matrix M as follows:

$$M = \left(\begin{array}{c|ccc|c} M_{0,0}^{T,T} & \ldots & M_{0,j'}^{T,P_{k'}} & \ldots & M_{0,N_P}^{T,P_N} \\ \hline \vdots & \ddots & \vdots & \ddots & \vdots \\ M_{j,0}^{P_k,T} & \ldots & M_{j,j'}^{P_k,P_{k'}} & \ldots & M_{j,N_p}^{P_k,P_N} \\ \vdots & \ddots & \vdots & \ddots & \vdots \\ M_{N_p,0}^{P_N,T} & \ldots & M_{N_p,j'}^{P_N,P_{k'}} & \ldots & M_{N_p,N_p}^{P_N,P_N} \end{array}\right), \tag{8}$$

with

$$M_{0,0}^{T,T} = \sum_{i=1}^{N} \langle T_i|V^P|T_i\rangle, \tag{9}$$

$$M_{0,j'}^{T,P_{k'}} = \left(\langle T_{k'}|V^T\left|P_{j'}^v\right\rangle + \sum_{i\neq k'}^{N}\langle T_i|V^P|T_i\rangle\left\langle T_{k'}\right|P_{j'}^v\rangle\right) \times e^{-i(E_{j'}+\frac{1}{2}v^2-\varepsilon_0)t}, \tag{10}$$

$$M_{j,0}^{P_kT} = \left(\left\langle P_j^v\right|V^P|T_k\rangle + \sum_{i\neq k}^{N}\left\langle P_j^v\right|T_k\rangle\langle T_i|V^P|T_i\rangle\right) \times e^{-i(\varepsilon_0-E_j-\frac{1}{2}v^2)t} \tag{11}$$

$$M_{j,j'}^{P_kP_{k'}} = \left(\sum_{i\neq k'}^{N}\langle P_j^v|T_k\rangle\,\langle T_i|V^P|T_i\rangle\left\langle T_{k'}\right|P_{j'}^v\rangle + \left\langle P_j^v\right|T_k\rangle\langle T_{k'}|V^T\left|P_{j'}^v\right\rangle\right) \times e^{-i(E_{j'}-E_j)t}. \tag{12}$$

In the equations above $|T_i\rangle$ represents $|\phi_i^T\rangle$, $|P_j^v\rangle \equiv |\phi_j^P e^{i\mathbf{v}\cdot\mathbf{r}}\rangle$ is the ETF-augmented projectile state, j,j' are running over N_P, the number of projectile states, and k,k' over N, the number of sites on graphene. The matrix elements of the overlap S can be deduced from Eqs. (9) to (12) by replacing V^T and V^P by $1/N$. Note that this approach reduces to the ion-atom ($N = 1$ peculiar case) close-coupling equations and that the extra terms such as $\sum_{i\neq k}^{N}\langle P_j^v|T_k\rangle\langle T_i|V^P|T_i\rangle$ are responsible for the collective effects included in the model.

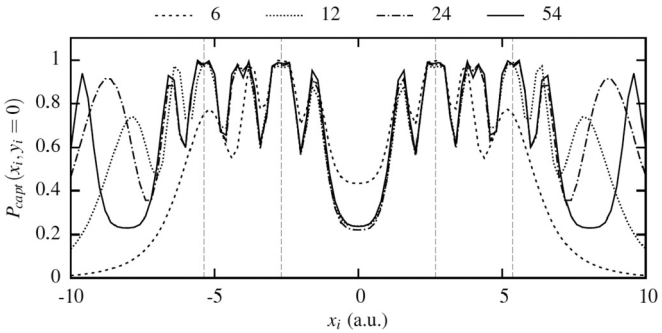

FIG. 2. Total capture probability $P_{\mathrm{capt}}(x_i, y_i = 0)$ along the x axis for $N = 6$, 12, 24, 54 centers on graphene sheet. The atomic positions along the x axis at $y_i = 0$ are represented by dashed gray vertical lines. The impact energy is 7.5 keV.

The results shown in the next section stem from this model where the variational parameter in the model potential [Eq. (3)] is set as $\alpha = 1.20$ to bind the outermost π electron with an energy $\varepsilon_0 = -0.22$ a.u. and described by a $2p_z$ Gaussian-type orbital with an exponent equal to 0.37, in agreement with static quantum chemistry calculations of graphene [25]. The computations require to evaluate the matrices S, M [Eqs. (8) to (12)] and to solve the coupled differential Eq. (7) for the expansion coefficients to obtain the capture probability, $P_{\mathrm{capt}}(x_i, y_i) = \sum_{k=1}^{N}\sum_{j=1}^{N_p}|c_j^k(t\to+\infty)|^2$ for a given velocity v and impact parameter $\mathbf{b}$ defined by the impact point coordinates (x_i, y_i), cf. Fig. 1. The computation time scales approximatively as $(N \times N_p)^2$: to test the convergence with respect to the number N of carbons on graphene, we performed computations with $N = 6$, 12, 24, and 54 (see Fig. 1), and included the dominant $H(n = 1)$ and $H(n = 2)$ capture states, as well as the $H(3s)$ and $H(3p)$ states.

In Fig. 2 the total capture probability P_{capt} along the x axis for $y_i = 0$ is presented for $N = 6$, 12, 24, and 54 sites. The four series of results demonstrate the convergence of the computations already for $N = 12$ sites for the capture probabilities pattern in the central hexagon (located between the two central vertical lines, $|x| \leqslant 3$). We shall therefore show and discuss the results stemming from $N = 12$ sites calculations since they can be considered as converged for the atoms of the central hexagon. The strong depletion of probabilities observed in the middle of the hexagons and already present in $N = 6$ calculations will be discussed in the following.

C. Model limitations

We here summarize the strengths and weaknesses of the present theoretical approach. The upside of the model stems from the sophisticated nonperturbative description of electronic processes occurring during an ultrafast (subfemtosecond) interaction: The transfer of a single electron from an almost infinite target to a swift proton is described with an extension of a state-of-the-art approach available in

atomic and molecular collision physics. The description of the final state part of the Hilbert space is therefore superior to what can be expected from TDDFT approaches. On the downside, our model encompasses a rather crude description of the static electronic structure of graphene. These limits are mainly two-fold since our model does not include (i) the σ-bond electrons, (ii) a Block-like formalism and electron delocalization. Furthermore, target excitation or ionization and multi-electronic processes are also neglected in the basis set expansion Eq. (4).

Concerning this last limitation, we expect that the cross sections of these reaction channels, perhaps with the exception of target excitation, will be very small as compared to the main channel—capture from the highest occupied p_z orbitals—for the considered impact energy. Indeed scattering events are then dominated by near-resonant capture, excitation, ionization, or double capture requiring more important energy transfers. For the same reason the transfer of the more bound σ electrons should be somewhat weaker since involving larger energy transfer (e.g., in $H^+ - C$ collisions capture from $2s$ is three times smaller than from $2p$, see Ref. [21]). Transfer of the π electrons to the proton will then dominate the scattering and prohibit additional σ electrons to be transferred. However, taking into account these electrons should not weaken the imaging capacity of the proposed scheme since they are localized between two neighboring C atoms so that their transfer to the proton should also present strong spatial selectivity. Finally, concerning the delocalization of the electrons, the hopping is a slower process compared to the interaction time required for the capture to occur so that it is a rather safe approximation to block this mechanism during the scattering event. In other words, the important physical properties of graphene that our model does not describe cannot significantly interfere with the collisional outcomes.

The extension of our model to include other processes, including multi-electronic ones, and to describe lattice periodicity with proper Bloch functions instead of our *ad hoc* approach should require severe developments, as the inclusion of several electrons in the Hamiltonian, Eq. (2), and numerous multihole bound (and continuum) states in the scattering wave function, Eq. (4). In summary, while we believe the present model captures the proper physics of single electron transfer to the proton, it may evidently be improved along the lines indicated here. Such improvements will expectedly not distort the contrast of the new imaging technique here proposed.

III. RESULTS AND DISCUSSION

Figure 3 shows the total electron capture probability P_{capt} for an impact energy of 7.5 keV and a continuous uniform distribution of proton impact points in the graphene plane modeled with $N = 54$ C atoms. We observe a large capture probability close to unity around the C atoms and a sharp drop to a minimum, almost vanishing probability, in the middle of the hexagons, see also Fig. 2. The capture probability surface is seen to be in good agreement with the initial state density. This strong sensitivity to the ion impact point suggests that capture measurements of a focused ion beam will also reflect disorder. In the right panel we display the capture probability in a situation where one C atom has been removed at the position

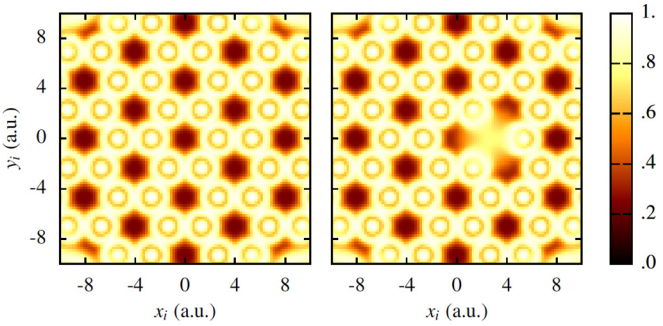

FIG. 3. (Color online) Left panel: Total electron capture probability $P_{\text{capt}}(x_i, y_i)$ from a continuous distribution of H^+ impact points on a semi-infinite periodic graphene surface at H^+ energy 7.5 keV. Right panel: Same as left with a vacancy (missing lattice carbon atom) located at $x = 2.68$, $y = 0$.

$(x, y) = (2.68, 0)$. This results in a lower probability in this region as a general distortion of the ordered probability pattern and therefore demonstrates the selectivity of this yield to image the presence of vacancies, doping atoms or crystallographic defects in two-dimensional materials.

In Fig. 4, we show the average capture probability resulting from a sampling of a large number of uniformly distributed impact points (x_i, y_i) in the central hexagon (with an $N = 12$ graphene sample) as a function of ion energy. We observe that the probability is almost unity up to 30 keV. When comparing to capture from a single C atom [21], the average transfer probability remains large for a much wider energy range, which shows that single capture from graphene is a multicenter—collective—event from low energy towards 50–100 keV. At the lowest energies the $H(2p)$ state is the dominating final capture state while the $H(1s)$ state increases in importance with energy and becomes the dominant one beyond 3 keV. This mechanism is related to the optimal overlap of the target and projectile wave functions in momentum space and is well known as the *velocity-matching* criterion in ion-atom collisions [26,27]. Capture to $H(n = 3)$ and higher states are always one order of magnitude smaller.

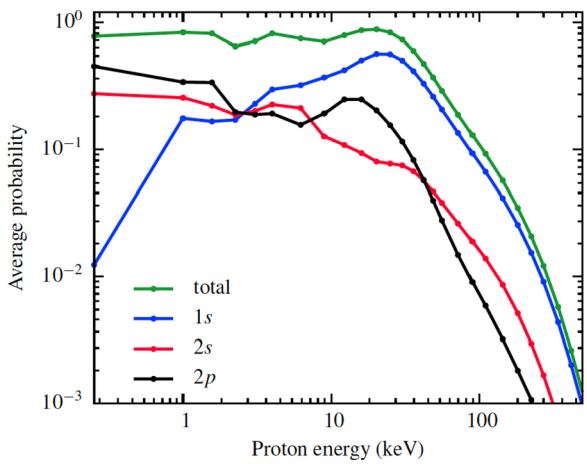

FIG. 4. (Color online) Average capture probability following a uniform perpendicular beam penetrating the graphene sheet against H^+ energy.

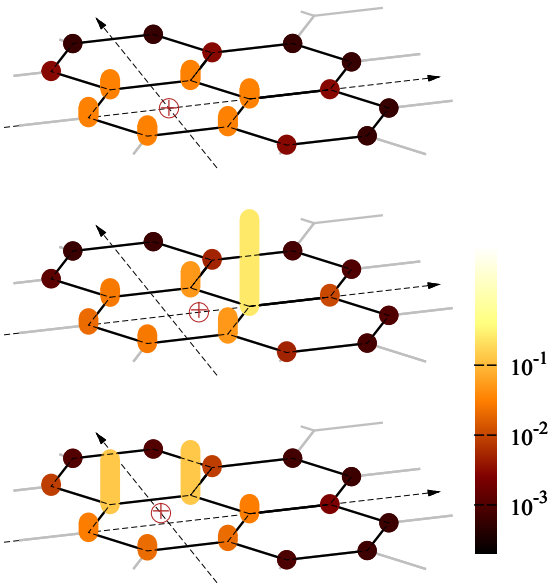

FIG. 5. (Color online) Distribution of capture probabilities $P^k_{\rm capt}(x_i, y_i)$ (cf. text) at 7.5 keV following ion impact at three different impact parameters (depicted by $\bigoplus$): top, $x_i = 0, y_i = 0$; middle, $x_i = 1, y_i = 0$; bottom, $x_i = 0, y_i = 1$.

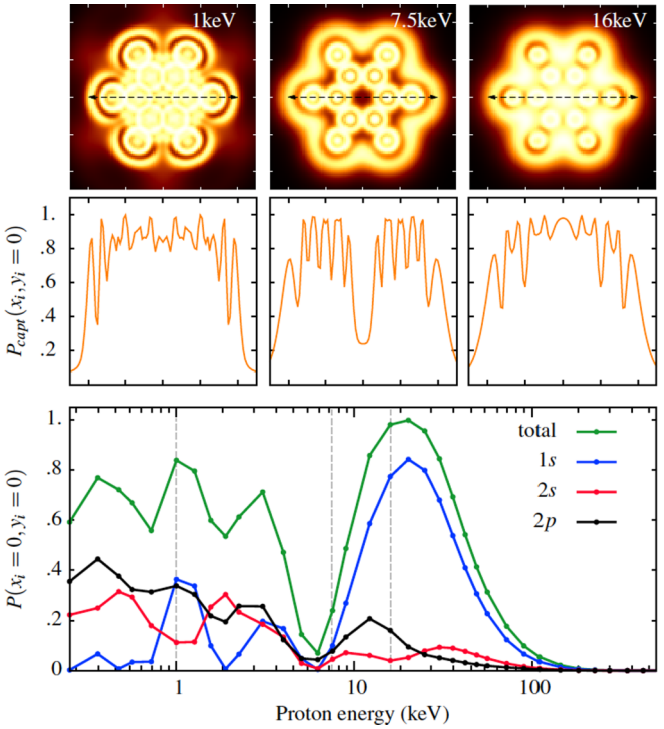

FIG. 6. (Color online) Upper panels: total capture probability $P_{\rm capt}$ profile in the xOy plane compared for three different projectile energies. Middle panels: total capture probability $P_{\rm capt}$ along the x axis at $y_i = 0$ (following the dashed lines in the upper panels). Lower panel: total and sub-shell capture probabilities at the center $(x_i = 0, y_i = 0)$ of the hexagon against projectile kinetic energy.

To display how many atoms actually contribute to capture at selected proton impact points we show in Fig. 5 the site-selective capture probability $P^k_{\rm capt}(x_i, y_i) = \sum_{j=1}^{N_p} |c^k_j(t \to +\infty)|^2$ for three H^+ impact points (x_i, y_i). We observe a strong contribution from the nearest atoms and the next-nearest ones within the honeycomb lattice where the ion penetrates; from the neighboring lattices the contributions drop by about two orders of magnitude. Thus, the sharp surface image of Fig. 1 is rather puzzling in view of the rather nonlocal nature of charge transfer.

The image effect observed at 7.5 keV can be explained by destructive quantum interferences in a very narrow velocity region. This can be seen in the lower panel of Fig. 6 where the capture probability ($N = 12$ sites calculations) for impact at the center of the hexagon $P_{\rm capt}(x_i = 0, y_i = 0)$ is displayed as a function of H^+ energy: The two dominant $n = 2$ and the $n = 1$ contributions reach a global minimum around the 4–8-keV region. As a result, the top middle panel (7.5 keV) of the figure displays a clear surface image while the similar probability maps at 1 and 16 keV (left and right, top and middle panels in Fig. 6) results in a more complicated surface structure which has limited imaging capability. We should finally stress that the atom and shell selectivity of electron capture processes upon impact energy [23] opens the possibility to detect also an efficiently single dopant atom in the lattice. Indeed capture cross sections may be different by up to 50% for neighbor elements, such as C, N, and O, cf. Refs. [21,28,29], but also time-of-flight (TOF) detection which measures that the Q value of a transition can discriminate between these atoms using their respective energetic signature.

In the following the mechanism behind the minimum located in the middle of the hexagons at 7.5 keV energy will be studied within a simple model of the capture probability for a multicenter system. First, it is pointed out that the effect is not due to interferences between the final $H(n = 2)$ and $H(1s)$ states: Indeed reduced basis-state calculations with only a single capture state on H reproduce the same effects as those in Fig. 6. The minimum therefore has to originate from the geometry of the lattice and the equal strengths experienced by the capture state from the six nearest-neighbor C atoms when the ion passes through the honeycomb center.

In Fig. 7, the $H(1s)$-capture probability pattern on the xOy plane is displayed for six graphene-like C_N ($N = 1$–6) structures: When comparing the single atom ($N = 1$, i.e., ion atom) case to the five other multicenter ones, a gradual buildup of the probability depletion in the center of the structure is clearly observed. An incoherent superposition of single atom results cannot explain the strong decrease of capture probability, which should therefore be generated by collective effects taken into account in our model. Thus, destructive interference effects related to a collective probability flux from the different neighboring atoms to the projectile passing through the central region of the hexagons of graphene is needed to explain the probability minimum observed in Fig. 3.

The essence of this effect observed at the center of each hexagon can be grasped by a model that includes N dominantly populated capture (single hole) states, Φ^{Tk}_j [cf. Eq. (6)], which couple to the single target state Φ_0 with no vacancy. The most likely projectile states ϕ^P_j are the $1s$, $2s$, and $2p_0$ states (labelled by f in the following), which present cylindrical symmetry with respect to the Oz axis ($m = 0$). At the center

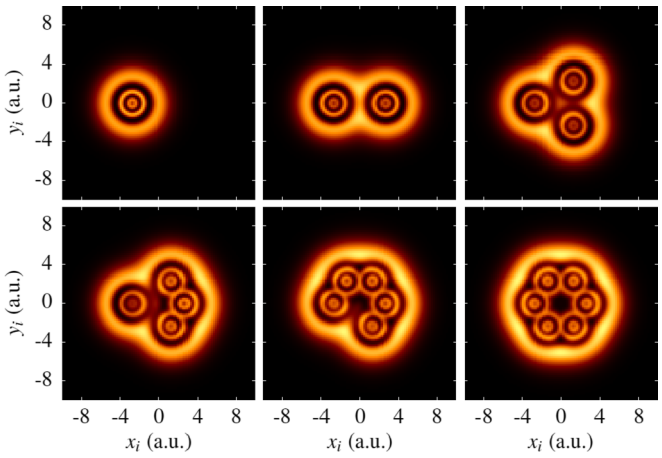

FIG. 7. (Color online) $H(1s)$-capture probability $P_{1s}(x_i, y_i) = \sum_{k=1}^{N} |c_{1s}^{k}(t \to +\infty)|^2$ profile for, respectively, an $n = 1$ to 6 C_n graphene-like structure. The impact energy is 7.5 keV.

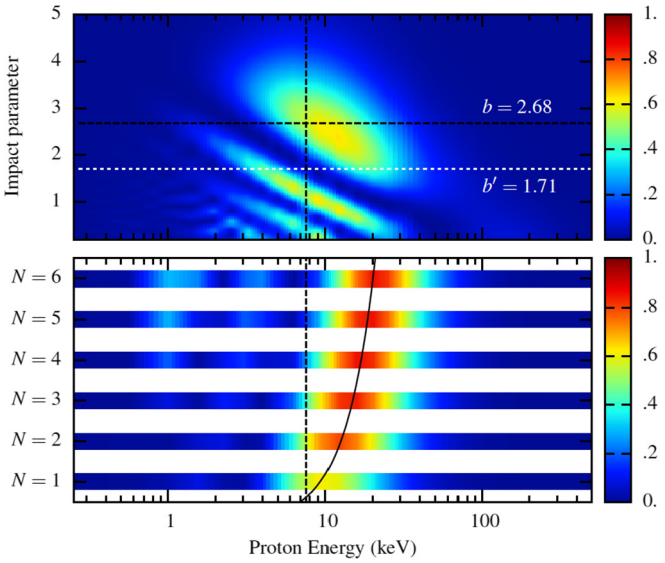

FIG. 8. (Color online) Top panel: $H(1s)$-capture probability as function of impact parameter and energy for H^+-C($2p_z$) collisions. The two horizontal lines mark two values of impact parameter: $b = 2.68$, which corresponds to impact at the center of hexagon with respect to the six nearest atoms and the scaled value $b' = b\,6^{-1/4}$, cf. text. The vertical line marks the optimal impact energy $E = 7.5$ keV (also shown in the lower panel) for vanishing probability at the center of the hexagon ($N = 6$). Bottom panel: $H(1s)$-capture probability at the center of a hexagon ($x_i = y_i = 0$, i.e., at a distance of 2.68 apart from the six closest carbons) as a function of impact energy for $N = 1$ to six-center target structures, cf. Fig. 7 for the respective geometries. The solid black line connects the maximum of probability for the six cases and shows the $N^{3/7}$ energy scaling discussed in the text.

of a hexagon these capture states with a single vacancy on a given C labelled k are therefore characterized by probability amplitudes $c_f^k(t)$, which have equal value (magnitude and phase) for the six centers due to the symmetry. In this condition the dynamics reduces to the coupling between two eigenstates:

$$\Psi = c_0(t)\,\Phi_0\,e^{-i\,N\varepsilon_0 t} + c_f(t)\,\bar{\Phi}_j^N\,e^{-i\left((N-1)\varepsilon_0 + \mathrm{E}_j + \frac{1}{2}v^2\right)t}, \quad (13)$$

with Φ_0 the initial state and $\bar{\Phi}_f^N$ a particular symmetric entangled N-center state, $\bar{\Phi}_f^N = \frac{1}{\sqrt{N}} \sum_{k=1}^{N} \Phi_f^{Tk}\,e^{i\mathbf{v}\cdot\mathbf{r}_k}$.

It should be noted that this later example can be identified in cold atom physics as the so-called Rydberg blockade state, which describes the excitation of precisely one electron in an ensemble of cold atoms exposed to a correctly tuned laser. In this particular case the collective effect stems from the large dipole moments of Rydberg atoms [30,31]. Due to this effect only a single electron in the final excited state can be achieved within a definite volume of a cold atomic gas containing N atoms. In other words, as soon as one electron excitation is achieved the large dipole moments of the excited complex sets up a detuning which causes multiple excitations to be far off resonance. Since all N atoms contribute on equal footing to the initial excitation an N-electron entangled state is obtained.

In the present case, the blockade is setup by the restriction of electron capture of a single electron while all lattice target atoms involved in the capture process takes part in creating the entangled single eigenstate $\bar{\Phi}_f^N$. The remaining $N - 1$ states following diagonalization become a set of "dark" states which decouple from the initial state and thus remain unpopulated during the projectile passage. It may be noted that for multiply charged projectiles the capture of several electrons is likely to take place, resulting in entangled "multihole" states.

The expression of the dynamics within these two active states, cf. Eq. (13), results in a set of two coupled differential equations for coefficients $c_0(t)$ and $c_f(t)$. To highlight the main effects of the symmetry and the blockade upon capture approximated differential equations can be derived by neglecting the overlaps between target and projectile states [Eqs. (8) to (12)]. Using standard phase transformations to remove the diagonal matrix elements (see, for example, Ref. [32]), the coupled differential equations can be expressed as

$$i\frac{d}{dt}\begin{pmatrix}\bar{c}_0\\ \bar{c}_f\end{pmatrix} = \begin{pmatrix}0 & \sqrt{N}V\\ \sqrt{N}V^* & 0\end{pmatrix}\begin{pmatrix}\bar{c}_0\\ \bar{c}_f\end{pmatrix}, \quad (14)$$

where $V \equiv V(R)$ represents the time-dependent Coulombic matrix elements between the initial state and the final capture state and the probability amplitudes $\bar{c}_{0/f}(t) \approx c_{0/f}(t)$ depend upon the impact parameter and velocity. From this simple model one can observe a $\sqrt{N}$ scaling of the coupling between the initial state and the final capture state: In other words for central impact the projectile can be regarded as carrying an effective charge $\alpha = N^{1/2}$ when going from one-center target (ion-atom) to N-center target collisions. Using the low-energy limit (near constant capture, as illustrated in Fig. 4) of the Bohr-Lindhard classical model [33,34] and a standard Monte Carlo scheme for integration, the impact parameter can be scaled at a given velocity so that $P_f^{(N)}(\alpha^{1/2}b, v) = P_f^{(1)}(b, v)$. In this simple model the capture probability for the N-center target can then be deduced from the ion-atom case by shifting the impact parameter with a factor $\alpha^{-1/2} = N^{-1/4}$, as the projectile was effectively passing closer to the centers when impacting an N-atom structure.

The validity and the limits of the model are illustrated in Fig. 8 with a set of results stemming from the full coupled-channel calculations, Eqs. (7) to (12): In the lower panel the dependence of the $H(1s)$-capture probability upon impact energy is presented for the center ($x_i = y_i = 0$) of

one- to six-center structures (see Fig. 7) while the upper panel displays the corresponding probability "v,b-landscape" of the ion-atom case ($N = 1$). The scaling in the impact parameter is clearly shown at the optimal energy 7.5 keV with the shift from high to low probabilities when increasing the number of centers, as the impact parameters decrease from 2.68 (close to the probability maximum for $N = 1$) to $1.71 = 2.68\ 6^{-1/4}$ (valley region). This simple model does demonstrate the high-contrast image observed for the graphene at 7.5 keV in the previous figures. It is also interesting to mention, finally, that the high velocity limit (v^{-7} decrease of capture) of the Bohr-Lindhard model allows to derive a scaling rule with respect to the impact velocity v at a given impact parameter $P_f^{(N)}(b,\alpha^{3/7}v) = P_f^{(1)}(b,v)$. This is equivalent to a shift by $N^{3/7}$ of the energy for equivalent probability: This is illustrated in the bottom panel of Fig. 8 by the solid line connecting the maximum capture probabilities, from $N = 1$ to 6. On the other hand, the limit of the model is also illustrated since it cannot account for the increase of capture probability along this $N^{3/7}$ curve. Indeed the coupling matrix elements related to collective effects have been removed in the model [Eq. (14)] when neglecting target-projectile overlap.

In conclusion, the entanglement between the multi-electron one-hole target state on the different C atoms of a graphene hexagon explains qualitatively the minimum of the probability observed at the center of the structure, and therefore the contrast of the images. This model shows also the dependance of the optimal energy upon the considered structure, which can be inferred from the knowledge of the corresponding $N = 1$ structure. When considering noncentral proton passages through the honeycomb cell the process may be described approximatively by a direct extension of the model by introducing hole-site-dependent couplings V_i in Eq. (14), the distances between the considered impact point and the closest C atoms being then nonequivalent. The decreased symmetry when departing from the common coupling makes automatically more projectile eigenvectors to couple to the initial state. Thus, as observed, the capture probability can be expected to increase for noncentral proton passage for the energy corresponding to a minimum at the center of symmetry of the honeycomb cell.

Note finally that Eq. (14) can be simplified even further by setting the matrix element V constant in a given finite collision time $T_{\rm coll}$ (or region $Z_{\rm coll} = v\ T_{\rm coll}$) and zero outside: This usual simple prescription in atomic collisions gives a capture probability proportional to $\sin^2(\sqrt{N}\ V\ T_{\rm coll})$. Thus, from the significant transfer probability for $N \sim 1$ or 2, increasing the number of target atoms to 6 will lead to a vanishing capture probability for certain optimal collision times. This explains also qualitatively the oscillatory behavior of the $H(1s)$ capture probability in Fig. 6 as well as the single oscillation for the $H(n = 2)$ states with a different effective coupling constant V and collision region $Z_{\rm coll}$.

IV. CONCLUSION

In conclusion, a multicenter multi-electron coupled-channel model for the description of charge transfer in the nondestructive interaction between ions and monolayer materials has been developed and applied to proton-graphene collisions. Our calculations show that single electron capture to a focused proton beam penetrating a single surface layer yields probabilities which provide a contrasted image of the surface structure within a unique and narrow projectile energy region. We demonstrate that the contrast observed for central lattice penetration of the ion can be deduced from an entangled multi-electron single-hole state. For optimal impact energy the image is formed by a coherent contribution from the $N \gg 1$ neighboring atoms for each projectile impact point on the surface. This scheme is therefore geometry and atomic highly selective. As such, we have presented the principles of a new imaging technique based on an entirely different mechanism in comparison to the generation of secondary electrons used in the HIM technique.

ACKNOWLEDGMENTS

We thank Stian Sørngard for providing the graphene image in Fig. 1 and the referees for stimulating discussions on the validity and limitations of the model. The research is supported by the French-Norwegian bilateral Aurora program.

[1] A. K. Geim and K. S. Novoselov, Nat. Mat. **6**, 183 (2007).
[2] K. Yu, P. Wang, G. Lu, K.-H. Chen, Z. Bo, and J. Chen, J. Phys. Chem. Lett. **2**, 537 (2011).
[3] S. Huber, T. Hell, M. Probst, and A. Ostermann, Theor. Chem. Acc. **132**, 1 (2013).
[4] O. Leenaerts, B. Partoens, and F. M. Peeters, Phys. Rev. B **77**, 125416 (2008).
[5] I. Radović, D. Borka, and Z. L. Mišković, Phys. Rev. B **86**, 125442 (2012).
[6] S. A. Sørngård, S. I. Simonsen, and J. P. Hansen, Phys. Rev. A **87**, 053803 (2013).
[7] V. V. Kulagin, V. A. Cherepenin, Y. V. Gulyaev, V. N. Kornienko, K. H. Pae, V. V. Valuev, J. Lee, and H. Suk, Phys. Rev. E **80**, 016404 (2009).
[8] O. Lehtinen, J. Kotakoski, A. V. Krasheninnikov, and J. Keinonen, Nanotechnology **22**, 175306 (2011).
[9] A. V. Krasheninnikov, Y. Miyamoto, and D. Tománek, Phys. Rev. Lett. **99**, 016104 (2007).
[10] S. Mathew, T. Chan, D. Zhan, K. Gopinadhan, A.-R. Barman, M. Breese, S. Dhar, Z. Shen, T. Venkatesan, and J. T. Thong, Carbon **49**, 1720 (2011).
[11] G. Compagnini, F. Giannazzo, S. Sonde, V. Raineri, and E. Rimini, Carbon **47**, 3201 (2009).
[12] J. M. Raimond, M. Brune, and S. Haroche, Rev. Mod. Phys. **73**, 565 (2001).
[13] S. Bubin, B. Wang, S. Pantelides, and K. Varga, Phys. Rev. B **85**, 235435 (2012).
[14] H. Zhang, Y. Miyamoto, and A. Rubio, Phys. Rev. Lett. **109**, 265505 (2012).
[15] B. W. Ward, J. A. Notte, and N. P. Economou, J. Vac. Sci. Technol. B **24**, 2871 (2006).

[16] D. Fox, Y. B. Zhou, A. O'Neill, S. Kumar, J. J. Wang, J. N. Coleman, G. S. Duesberg, J. F. Donegan, and H. Z. Zhang, Nanotechnology **24**, 335702 (2013).
[17] T. Royer, D. Dowek, J. C. Houver, J. Pommier, and N. Andersen, Z. Phys. D - Atoms, Molecules and Clusters **10**, 45 (1988).
[18] V. Véniard, R. Taïeb, and A. Maquet, Laser Phys. **13**, 465 (2003).
[19] W. Fritsch and C. D. Lin, Phys. Rep. **202**, 1 (1991).
[20] J. Caillat, A. Dubois, I. Sundvor, and J.-P. Hansen, Phys. Rev. A **70**, 032715 (2004).
[21] P. C. Stancil, J.-P. Gu, C. C. Havener, P. S. Krstic, D. R. Schultz, M. Kimura, B. Zygelman, G. Hirsch, R. J. Buenker, and M. E. Bannister, J. Phys. B-At. Mol. Opt. **31**, 3647 (1998).
[22] M. S. Gravielle and J. E. Miraglia, Phys. Rev. A **44**, 7299 (1991).
[23] B. H. Bransden and M. R. C. McDowell, *Charge Exchange and the Theory of Ion-Atom Collisions* (University Science Books, Sausalito, CA, 1983).
[24] D. A. McQuarrie, *Quantum Chemistry* (Oxford University Press, New York, 1992).
[25] S. I. Simonsen, S. A. Sørngard, M. Førre, and J. P. Hansen, J. Phys. B: At. Mol. Opt. Phys. **47**, 065401 (2014).
[26] E. E. B. Campbell, I. V. Hertel, and S. E. Nielsen, J. Phys. B-At. Mol. Opt. **24**, 3825 (1991).
[27] E. Y. Sidky and H.-J. T. Simonsen, Phys. Rev. A **54**, 1417 (1996).
[28] R. Cabrera-Trujillo, Y. Öhrn, E. Deumens, and J. R. Sabin, Phys. Rev. A **62**, 052714 (2000).
[29] T. Kirchner, H. J. Lüdde, M. Horbatsch, and R. M. Dreizler, Phys. Rev. A **61**, 052710 (2000).
[30] E. Urban, T. A. Johnson, T. Henage, L. Isenhower, D. D. Yavuz, T. G. Walker, and M. Saffman, Nat. Phys. **5**, 110 (2009).
[31] A. Gaëtan, Y. Miroshnychenko, T. Wilk, A. Chotia, M. Viteau, D. Comparat, P. Pillet, A. Browaeys, and P. Grangier, Nat. Phys. **5**, 115 (2009).
[32] A. Dubois, J. P. Hansen, and S. E. Nielsen, J. Phys. B **22**, L279 (1989).
[33] N. Bohr and J. Lindhard, K. Dan. Vidensk. Selsk. Mat. Fys. Medd. **28**, 7 (1954).
[34] H. Knudsen, H. K. Haugen, and P. Hvelplund, Phys. Rev. A **23**, 597 (1981).